Journal of Catalysis **182,** 417–429 (1999)
Article ID jcat.1998.2388, available online at http://www.idealibrary.com on IDEAL®

The Correlation of Subsurface Oxygen Diffusion with Variations of Silver Morphology in the Silver–Oxygen System

Anton J. Nagy, G. Mestl, D. Herein, G. Weinberg, E. Kitzelmann, and R. Schlögl

Fritz-Haber-Institut der Max-Planck Gesellschaft, Faradayweg 4-6, D-14195 Berlin, Germany

Received July 22, 1998; revised November 16, 1998; accepted December 16, 1998

Silver undergoes pronounced morphological changes following high-temperature treatment in various gas atmospheres. SEM analysis shows that high-temperature treatment in oxygen leads to pronounced facetting of the silver surface. *In situ* **XRD shows a strong texturing of the polycrystalline bulk and an expansion of the unit cell resulting from the dissolution of oxygen. Two distinctly different forms of subsurface oxygen have been identified and the influence of morphological changes on the mechanism leading to their formation clarified. The first of these species is O_β. It is bulk-dissolved oxygen which diffuses via an interstitial mechanism through low-resistance diffusion paths such as grain boundaries and open crystalline planes. Temperature programmed desorption spectroscopy analysis reveals that high-temperature oxygen pretreatment results in the formation of crystalline surfaces exhibiting different oxygen diffusion barriers. At elevated temperatures, pure thermal reordering dominates over oxygen-induced restructuring of the silver bulk and surface. The near-surface region is, therefore, comprised primarily of close-packed crystalline planes at elevated temperatures. The barrier for interstitialcy diffusion is overcome at temperatures in excess of 923 K, allowing bulk-dissolved, atomic oxygen to (O_β) segregate into these low-indexed planes. This likely occurs via an interstitialcy diffusion mechanism where oxygen substitutes for silver atoms in the lattice. This oxygen species is referred to here as O_γ. Analysis of ISS depth profiling of silver foils treated under various conditions shows that the diffusion coefficient is a positive function of the oxygen concentration. This is a direct result of the oxygen-induced recrystallization of the silver resulting in a lowered barrier to diffusion.** *In situ* **XRD shows that oxygen located in octahedral holes of silver preferentially diffuses in the [110] direction. This requires the anisotropic displacement of silver atoms. The resulting strain culminates in a slight expansion of the silver unit cell and the preferential growth of crystals in the shape of needles. STM imaging of the surface shows the macroscopic silver facets to be composed of smaller, columnar crystallites, thus confirming the validity of the model based on the XRD data.** © 1999 Academic Press

Key Words: **electrolytic; silver; oxygen; diffusion; kinetics; defect structures; morphology; oxidation reactions; oxidative coupling of methane.**

I. INTRODUCTION

Silver is used, industrially, as a catalyst for the partial oxidation of methanol to formaldehyde (1, 2, 3) as well as for the oxidation of ethylene to ethylene epoxide (4). The high permeability of silver for oxygen and hydrogen also makes it an ideal material for membrane reactor and separation studies ($D_{H2,973\,K} = 2.82 \times 10^{-3}$ cm^2/s; $D_{O2,973\,K} = 8.19 \times 10^{-2}$ cm^2/s) (5, 6). The gas transport properties of silver show a strong dependence on morphology where both the bulk morphology and the terminating surface structure play an important role in the overall diffusion process (6, 7). Densely packed crystal structures exhibit increased diffusion resistance and significantly lower sticking coefficients for a variety of gases (5, 6, 8, 9). In addition, different crystalline structures exhibit varying degrees of diffusion anisotropy which may lead to a preferential channeling of the diffusing species in a particular direction (10). Therefore, both the diffusion *rate* and the *direction of propagation* are intimately linked with the types of crystalline structures present. Among these, defects play an important role in gas adsorption and diffusion in solids. Surface steps and kinks contain unsaturated bonds which may act as active sites for gas adsorption (11, 12). This is the first step in the diffusion process. In addition, grain-boundaries provide low-resistance diffusion paths for gas diffusion in the metal bulk (5, 6, 9, 10). High-temperature treatment of solids often results in changes in the concentration and nature of defects as well as surface and bulk-recrystallization (9–12). These morphological changes arise from the fact that the system is driven to achieve a minimization of the total free energy. The final orientation of a single-crystalline domain in an isochoral, isothermal system is, therefore, uniquely determined by that structure exhibiting the lowest free energy. This criterion determines the equilibrium surface structure as well as the 3-D crystal structure (Wolf Plot) (9–11). The ability of a solid to achieve its thermodynamically predetermined equilibrium state is, however, often limited by the kinetics of the solid-state reaction which often requires significant mass transfer. Surface transitions at the gas-metal interface often occur at significantly lower temperatures than bulk transformations (13). Bulk transitions typically require temperatures in excess of the Tamann temperature ($T_t = 0.5\ T_{melt}$) in order to produce structural changes within a reasonable time frame of interest (9–11). These changes in morphology may either be thermally induced or

0021-9517/99 $30.00

reaction-induced (11). Changes which are purely *thermally* induced occur with or without the presence of a reacting atmosphere. The process is driven in such a way as to result in a decrease of the surface-free energy. *Reaction*-induced morphological changes require the presence of a reacting atmosphere which results in the formation of structures different than those found after treatment in inert gas or vacuum. The reaction of a solid with highly reactive gas-phase radicals is typically assumed to be the dominant mechanism and is usually kinetically controlled. The mechanism of reaction-induced restructuring is a relatively poorly understood phenomenon which has received increased attention lately. A recent publication by Wei and Phillips (11) provides an excellent critique of literature on this topic.

Densely packed, low-indexed terminating crystal structures exhibit the highest degree of bonding and are therefore the thermodynamically preferred surface structures. Silver surfaces treated at elevated temperatures tend, therefore, to break up into a complex arrangement of crystal planes exhibiting a saw-tooth profile (9–11). This effect is known as faceting. Faceting only occurs for situations where the total faceted surface area *created* exhibits a lower total surface free energy than the *original* nonfaceted surface area. Faceting requires extensive mass transport of silver atoms via bulk and surface diffusion or via gas-phase transport resulting from sublimation and condensation. The facet formation mechanism, in the presence of oxygen, is believed to occur via a Stranski–Krastanov-type process (14) where bulk silver atoms migrate to the surface and then diffuse along the surface, eventually bonding to energetically favorable step or kink sites (9–11). The formation of facets via oxide formation is not very likely at the temperatures used in this study ($T > 923$ K) as the most stable oxide of silver, Ag_2O, decomposes thermally at 473 K. Broad terraces exhibiting monatomic steps initially result from thermal treatment in oxygen. These steps wander across the surface eventually resulting in an increased step height and density. A microscopically corrugated surface with features in the nm–μm size range results. These corrugations are referred to as facets. This microscopic structure typically shows a macroscopic periodicity in the μm size range. Given ample time, a surface consisting of an agglomeration of intersecting single-crystalline planes is formed.

A number of authors have shown that treating silver in an oxygen atmosphere may result in the formation of surface structures different than those formed during treatment in vacuum or inert gas (10, 11, 15). This phenomenon is believed to arise from adsorbate-induced changes in the surface free energy. Oxygen adsorption is known to result in a reduction in the surface free energy of solids (16). It is a well-known fact that oxygen adsorbs preferentially on the more open (coordinatively unsaturated) terminating crystal structures (sticking coefficients for oxygen on various crystalline planes (111)10^{-7}, (100)10^{-4}, (110)10^{-3} at room temperature) (6–8). These open crystal structures are, in the absence of adsorbates, thermodynamically unstable. A clean, high-indexed terminating surface contains a high density of dangling bonds which results in an elevated surface free energy (10, 11). Preferential adsorption of oxygen on these rough surfaces results in an adsorbate-induced decrease in the surface free energy. This, in turn, exerts a stabilizing influence leading to their subsequent growth. This is shown schematically in Fig. 1. Moderate temperatures and high oxygen pressures should, therefore, favor the formation of such structures. The steady-state morphology will, therefore, be determined by the equilibrium between pure thermal rearrangement and oxygen-induced reordering. This equilibrium is fixed by the temperature and partial pressure of oxygen in the system.

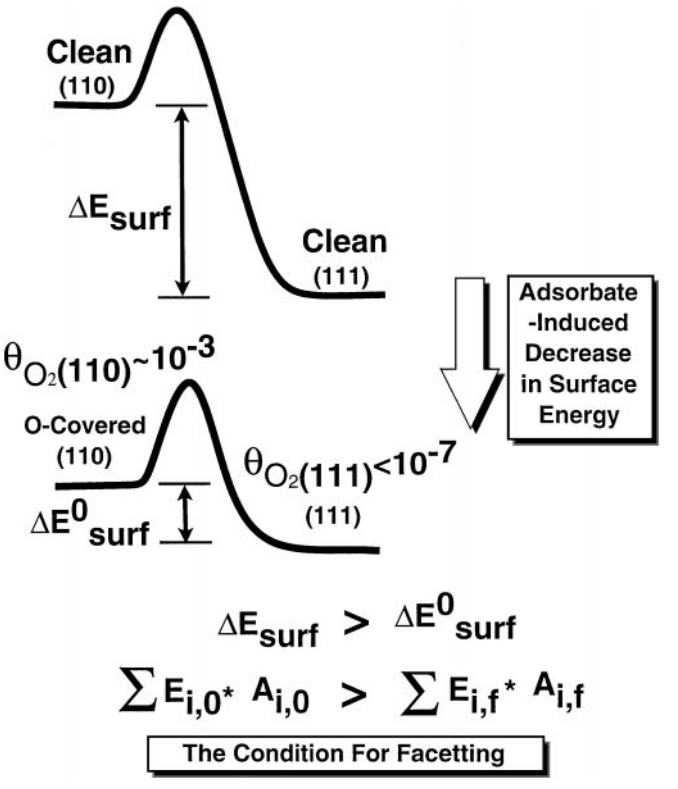

FIG. 1. The influence of oxygen coverage on the surface-free energy. The variation in energy potential of the silver (111) and (110) surfaces before and after oxygen adsorption.

It has been shown that two distinctly different oxygen species may be formed in the *subsurface* region of silver (14, 17–19). These species differentiate themselves in both their location and bonding states. They have previously been characterized with a variety of spectroscopic techniques (14–17, 20–25). The mechanism leading to the formation of these species is, however, poorly understood. In this paper, a model is proposed which allows for an understanding of the diffusion processes which ultimately lead to the formation of these various oxygen species. The first of these subsurface

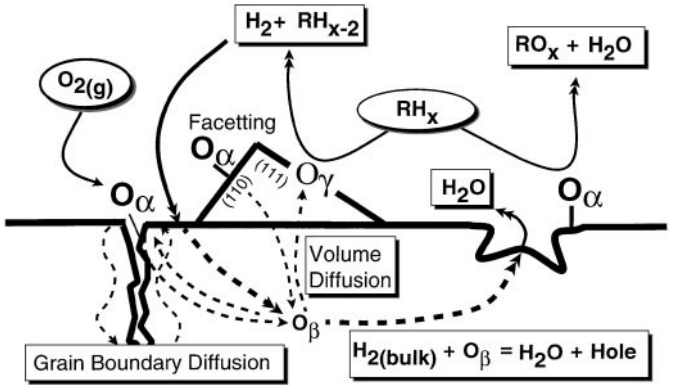

FIG. 2. Scheme of high temperature dehydrogenation over electrolytic silver (the role of subsurface oxygen). Proposed mechanism for the participation of subsurface oxygen in high-temperature reactions catalyzed by electrolytic silver.

species is known as O_β. This species is formed when dissociatively adsorbed, atomic surface oxygen (O_α) diffuses into the bulk. A second species, O_γ, is formed at higher temperatures ($T > 873$ K). It has been suggested that O_γ is formed via the segregation of O_β to the surface (14–17). The reasoning behind this mechanism is presented here. It is shown that the competing effects of thermal reordering and oxygen-induced restructuring result in the formation of different crystal structures with varying diffusivity. The extent of formation and nature of this restructuring shows a strong dependence on oxygen partial pressure and treatment temperature.

The partial oxidation of methanol and the oxidative coupling of methane (OCM) to C_2 hydrocarbons are two reactions which are believed to be catalyzed by O_γ (11, 13, 16). The assumption that the segregation of O_β to the surface region is necessary for O_γ formation implies that the kinetics of this step should play an important role in the overall reaction kinetics for reactions catalyzed by O_γ. This study lays the groundwork necessary for the development of a kinetic model which explains the role of O_β and O_γ reacting under steady-state reaction conditions. Subsurface oxygen is continuously produced via bulk dissolution and consumed via surface segregation and reaction. An outline of the proposed OCM mechanism is shown in Fig. 2.

II. EXPERIMENTAL SECTION

Materials

Oxygen (5.0), helium (5.0), and methane (3.5) were purchased from Linde and were used for pretreatments. Helium was purified with an Oxisorb column prior to use in reaction. A 99.999% pure silver foil purchased from Goodfellow was used for the XPS, SEM, and STM studies. Fine Ag powder was produced for the *in situ* XRD experiments by reducing a fine Ag_2O powder from Aldrich (99.9%) *in situ* with methanol (16 ml/min CH_3OH + 100 ml/min He). This method of *in situ* reduction produced a thin, polycrystalline layer supported on a stainless steel resistance heater. The *in situ* reduction was performed at 573 K. Oxidation was performed by flowing 100 ml/min O_2 over the sample. Methanol was not dried prior to use. Electrolytic silver was generously provided by the BASF AG and was used for the TDS runs.

XPS

The sample was cleaned by repeated cycles of oxidation (573 K, 100 mbar O_2), flashing (873 K), and pumping followed by Ar^+ sputtering (1 kV, 2 μA). Significant quantities of impurities ($C_{tot} < 5$ at%, Na < 2 at%, K < 1 at%) segregated to the surface upon heating. Two days of repeated sputtering cycles were necessary in order to obtain an acceptable purity. It is impossible to remove all of the impurities present. XPS was performed with a modified Leybold LHS 12 MCD system. The XPS spectra were obtained with Mg K_α radiation ($h\nu = 1253.6$ eV) using a fixed analyzer pass energy of 48 eV. This results in a resolution of approximately 0.1 eV and a depth of analysis of approximately 30 Å. Surface compositions were calculated after performing a Shirley background subtraction and were quantified using the respective atomic correction factors. ISS spectra were generated using a scanning, defocused 100 eV He^+ primary beam. The He^+ current was 1 μA which resulted in a flux of about 6×10^{12} ions/cm^2 s. All photoelectron spectra were recorded at 573 K in order to minimize interference from adsorbed carbon contamination. Temperature programmed desorption spectroscopy (TDS) and XPS were carried out in separate apparatuses as the available XPS facilities do not include the possibility of performing TDS.

SEM

SEM images were taken with a Hitachi S-4000 SEM equipped with an EDX for element identification. Samples were first polished with diamond paste and then treated for 1 min in an ultrasound bath of acetone in order to remove embedded diamond particles. Longer treatment times in the ultrasound bath led to severe deformation of the silver foil.

STM

STM images were taken with a Burleigh STM (model ARIS-3450) with a PID feedback controller which was interfaced with a PC. The tunneling voltage was 0.45 V and the current was 2.0 μA. Tips were cut to size and were made of Pt/Ir (80/20).

TDS

TDS measurements were made in an UHV chamber with an average background pressure of 3×10^{-8} mbar. The

vacuum was pumped by oil-free Balzer's turbopumps with a pump rate of 240 L/s. Analysis of the background gas shows water to be the primary impurity present. Monitoring of desorption products was made with a Hiden (Hal2) quadrupole mass spectrometer coupled to a Next workstation. A sampling rate of 0.65 scans/s was used. A water-cooled, infra-red oven was used for sample heating. The thermocouple (Type K) was placed immediately below the sample and was in direct contact with the quartz holding tube. Linear heating ramps from 373 to 1273 K with a maximum heating rate of 2.5 K/s were possible with this setup. The sample was treated in flowing oxygen (purity 5.0, 17 ml/min) at 973 K overnight in order to minimize problems arising from carbon contamination. The sample was subsequently transferred through air to the UHV setup. Oxidation–reduction cycles were performed until the CO_2 signal reached an acceptable level (approximately 2% of max O_2 signal). This cleaning procedure typically lasted one week. Dosing pressures for the temperature-programmed desorption experiments ranged from .01–300 mbar. Three dosing temperatures of 573, 773, and 973 K were used. All exposures were made for 5 min. Longer exposure times did not show an increased oxygen uptake for samples treated in excess of 573 K indicating rapid equilibration of the silver and gas. One gram of silver was used for all runs. The oxygen pretreatment temperatures are equal to or exceed the thermal desorption temperature of surface-bound atomic oxygen (O_α, $T_{des} = 573$ K). This, in combination with the fact that the unsupported silver samples have a very low surface area (<0.001 m^2/g) and a low sticking coefficient, means that surface-bound atomic oxygen, O_α, should not be observed for these runs. The sample was evacuated for 5 min prior to taking each TD spectrum. The fact that the spectra are not baseline resolved for runs made in excess of 10 mbar is due to the inability to completely pump off all of the oxygen within this time. The pumping time was held constant at 5 min prior to taking each TD spectrum as reaction with bulk-dissolved carbon results in CO_2 formation for longer holding times. It is also important to note that the extremely high dosing pressures used here ($P < 300$ mbar) are much higher than the Langmuir exposures typically used in surface-science experiments. These high pressures were chosen with the intention of approaching, as closely as possible, the actual reaction conditions used in the methanol oxidation reaction and the oxidative coupling of methane to C_2 hydrocarbons (1–10% O_2, total pressure = 1 bar).

XRD

A Stoe STADI P diffractometer using Cu K_α radiation and a Bragg–Brentano geometry was used for the powder diffraction measurements. This included a HOPG-secondary monochromator and a scintillation counter. *In situ* XRD was measured in a modified Bühler HTK 2.0 chamber. Measurements were made by taking the first point at room temperature and then heating in 100 K steps beginning at 373 K. The sample was allowed to equilibrate at the set temperature for 30 min prior to performing the measurement. The heating rate between steps was 10 K/min.

III. RESULTS AND DISCUSSION

SEM Analysis of Pretreated Foil

Figure 3a shows a micrograph of the surface of a polished silver foil subsequent to treatment in flowing He for 4 days. The surface consists of broad flat areas and shows very few grain boundaries. The high-temperature treatment has resulted in significant annealing of the surface. The surface is lightly faceted in some regions but is overwhelmingly flat and has a slightly "melted" appearance. Experiments made with He (5.0) without an "Oxisorb" filter show a completely faceted surface (not shown). It is absolutely critical, therefore, to use an inert gas of high purity when performing reference runs. The large discrepancy seen in the literature for work done on similar systems likely results from the presence of small amounts of O_2 impurities (13, 26–28). A quick calculation assuming a completely (111) faceted surface with a sticking coefficient of 10^{-7} shows that complete coverage should be reached in less than 30 min when using a 99.999% pure He stream. Most treatments performed in the literature lasted for days. Only a minimal amount of oxygen is, therefore, required to achieve monolayer coverage. The reference measurement in oxygen-free He clearly demonstrates that faceting occurs, at best, to a very small extent in the absence of oxygen.

Figure 3b is an image of the same foil after treatment for four days in oxygen at 1023 K. This treatment has resulted in massive morphological restructuring of the silver surface. The originally flat surface is now covered with pyramidal-like structures in the μm size range. It appears as if all structures located within a single crystalline area are oriented in the same direction indicating a preferential orientation of the single crystalline domains. Note that the orientations on opposite sides of the grain boundaries are typically different. Images at higher magnification show evidence of grain-boundary grooving (not shown). Previous work has shown the preferential crystallographic orientation of these surface structures to be a function of both oxygen pressure and treatment temperature (14).

Figure 3c shows an image of the foil subsequent to reaction in the oxidative coupling of methane for 4 days at 1023 K. The surface structures produced subsequent to oxygen pretreatment appear to be nearly identical to those formed during the OCM reaction. The unambiguous assignment of the exact crystallographic orientations of the facet faces is, unfortunately, not possible using SEM data alone. However, the similarity of the surface structures seen in Figs. 3b and 3c shows that a solid understanding of the

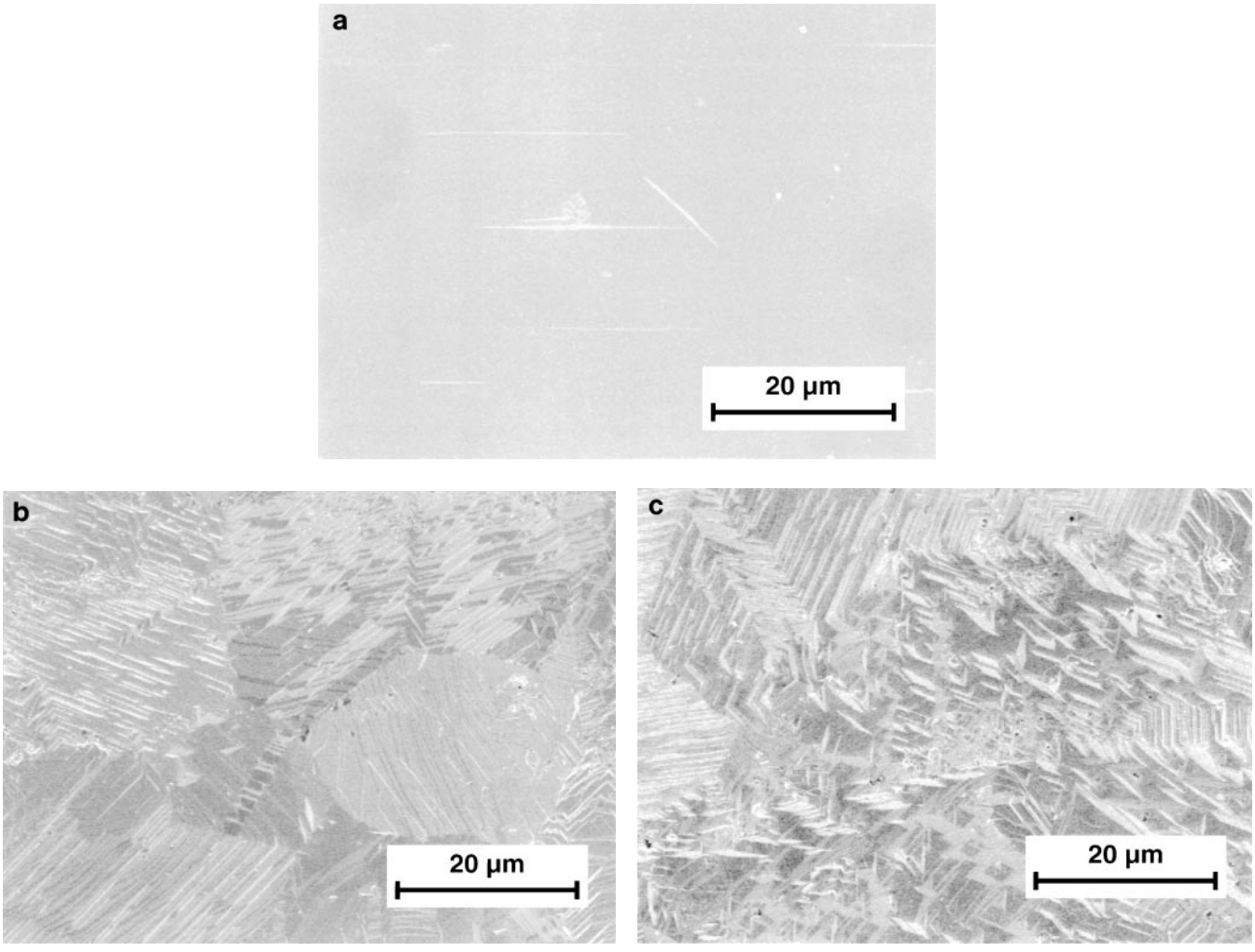

FIG. 3. (a) SEM image of a polycrystalline silver foil after treatment in flowing helium for 4 days, total volumetric flow rate 150 ml/min, 1023 K. (b) SEM image of a polycrystalline silver foil after treatment in oxygen for 4 days, 10% O_2 in flowing He, total volumetric flow rate 150 ml/min, 1023 K. (c) SEM image of a polycrystalline silver foil after use in the oxidative coupling of methane (OCM) reaction, 8.2 vol% O_2, 46 vol% CH_4, 45.8 vol% He, total volumetric flow rate 150 ml/min, 1023 K.

oxygen–silver interaction is essential to understanding the morphology–activity relationship for the silver-catalyzed OCM reaction.

TDS as a Tool for Studying Structural Changes

As stated in the Introduction, the formation of O_γ is believed to occur via the migration of bulk-dissolved oxygen (O_β) to the surface (14–17). The question then arises as to why surface segregation of bulk-dissolved oxygen should lead to the formation of an oxygen species exhibiting uniquely different chemical properties (O_γ) and not just to chemisorbed surface oxygen (O_α). The answer to this question lies in the intimate connection between thermal reordering of the silver metal and the dominant mechanism of oxygen diffusion in the silver bulk. Both are activated processes exhibiting an Arrhenius-type temperature dependence. A solid understanding of the kinetics of both of these processes is essential to elucidating the mechanism leading to the formation of O_γ. The strong structural dependence of gas diffusivity makes TDS a sensitive probe for studying morphological changes induced during the pretreatment. A thorough TDS investigation of the influence of oxygen pretreatment on the diffusive properties of oxygen in silver was therefore carried out with the goal of understanding the nature of the formation of both the O_β and the O_γ species.

Pretreatment at 573 K

Figures 4a–4c show oxygen–TD spectra for electrolytic silver samples pretreated in oxygen at various pressures and temperatures. A series of TD spectra obtained after having exposed the sample to various O_2 pressures at 573 K for 5 min are presented in Fig. 4a. The first broad, asymmetric peak centered at approximately 650 K is assigned

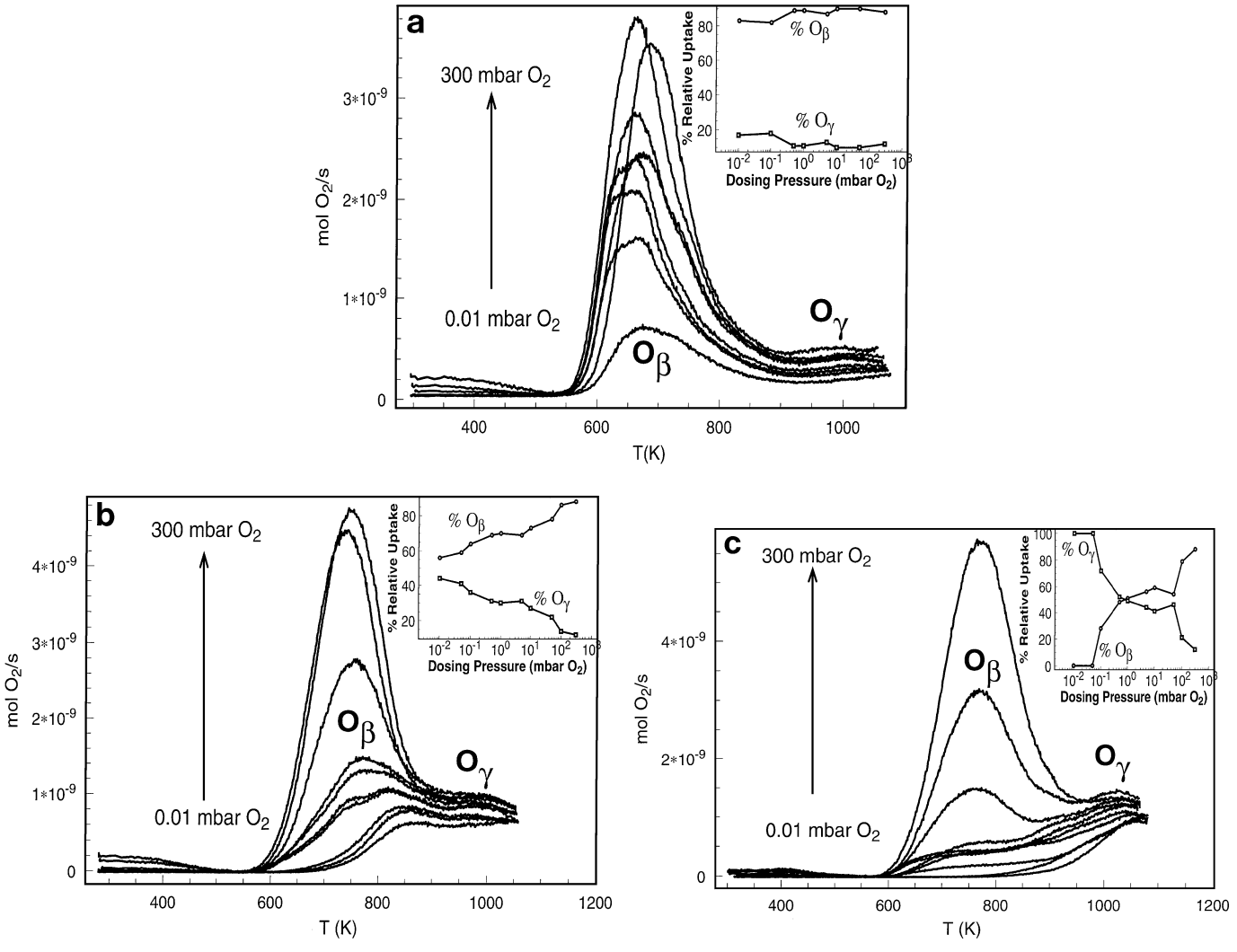

FIG. 4. (a) Oxygen thermal desorption spectrum of electrolytic silver pretreated in oxygen at 573 K. 1 g silver, 0.2- to 0.4-mm grain size, heating rate 1 K/s. (b) Oxygen thermal desorption spectrum of electrolytic silver pretreated in oxygen at 773 K. 1 g silver, 0.2- to 0.4-mm grain size, heating rate 1 K/s. (c) Oxygen thermal desorption spectrum of electrolytic silver pretreated in oxygen at 973 K. 1 g silver, 0.2- to 0.4-mm grain size, heating rate 1 K/s.

to O_β desorption. The weaker peak desorbing above 873 K is assigned to O_γ. The O_β signal results from diffusion and desorption of bulk-dissolved oxygen diffusing along low-resistance diffusion paths such as less closely packed crystal planes and grain boundaries. The broadness and asymmetry of this peak is to be expected as a polycrystalline silver sample offers a variety of paths for oxygen diffusion. A number of authors (3, 4, 7, 8, 11, 13–17) have assigned this species to bulk-dissolved oxygen. Two important pieces of evidence presented here support this. First, the signal does not saturate for dosing pressures made up to 300 mbar O_2. Second, the maximum calculated uptake for O_β of 6×10^{-7} mol O_2/g Ag would require about 30 multilayers assuming a completely (111) faceted surface with a surface area of 0.001 m^2/g and 100% coverage. The actual extent of (111) faceting and surface coverage (low probability of sticking: $\theta_{111} = 10^{-7}$) is probably much lower than this. In addition, it is a well-known fact that multilayer adsorption of oxygen on silver does not occur above room temperature (4, 7). The assignment of this peak to surface-bound oxygen is therefore impossible. Attempts at curve fitting fail as one may fit any number of curves of various line profiles. The point common to all of the diffusing species resulting in the O_β desorption peak is that the diffusion mechanism resulting in their formation likely occurs as a result of interstitial hole-jumping and/or grain boundary diffusion (5, 6, 9). This point will be touched upon again in the discussion.

The integral areas of both the O_β and the O_γ desorption signals increase for increasing dosing pressures. However, the O_γ signal increases only slightly. This hints that

it is probably confined to the near-surface region. The O_β desorption temperature in Fig. 4a shows a very weak dependence on the dosing pressure. The weak dependence of the desorption-temperature on exposure cannot simply be attributed to a first-order desorption of oxygen as the desorbing species originates from a bulk-dissolved species (O_β) (3, 4, 6–8, 14) which must first diffuse to the surface. The desorption rate is therefore limited by the diffusive flux of oxygen to the surface. Typical pre-exponential factors for the recombinative desorption of surface-bound atomic oxygen are typically on the order of 10^7–10^{15} (s^{-1}) (24, 29). Similar values for diffusion coefficients of oxygen in silver are between 10^{-1} and 10^{-3} s^{-1} (5, 6). The diffusion kinetics should, therefore, dictate the peak form as well as the desorption temperature. This is a critical point to be considered when interpreting thermal desorption spectra made under conditions where subsurface species are produced.

The O_γ desorption signal beginning at approximately 950 K is very weak. The inset in Fig. 4a shows the % value of the integrated O_2 desorption signal attributed to O_β and O_γ. There is no substantial variation in the relative integral desorption signals for both species. The insensitivity of the relative amounts of O_γ and O_β to dosing pressure at this temperature suggests that no significant morphological changes occurred during the pretreatment. SEM images show no faceting of the surface for Ag foils treated in oxygen at this temperature (data not shown). This observation is in agreement with observations made previously in the literature (24, 25).

Pretreatment at 773 K

Figure 4b shows that the situation is drastically different for oxygen pretreatments made at 773 K. Low-pressure dosing results in an O_β desorption maximum at 850 K. This is nearly 200 K higher than the desorption maximum for the identical dosing pressures seen in Fig. 4a. Subsequently increasing the dosing pressure results in a gradual shift of the O_β desorption peak maximum to lower temperatures. The O_β desorption maxima for high pressure doses ($P > 5$ mbar) is approximately 50 K higher than those obtained for the identical dosing pressures at 573 K seen in Fig. 4a. The weak desorption maximum for O_γ remains approximately constant for all dosing pressures. The desorption temperature for O_β remains constant for dosing pressures higher than 10 mbar. The relative amounts of O_β and O_γ formed subsequent to dosing at 773 K are shown in the inset of Fig. 4b. The relative amount of O_β increases monotonically and that for O_γ decreases monotonically. This behavior is very different from that which is observed in the inset of Fig. 4a for doses made at 573 K. The large variation in $\%O_\beta$ and $\%O_\gamma$ as a function of dosing pressure suggests that significant restructuring of the catalyst has taken place during pretreatment. This correlates well with the onset of faceting observed in the literature (24, 25).

Pretreatment at 973 K

Figure 4c shows a set of desorption spectra obtained after dosing at 973 K. There is a slight increase in the signal around 400 K. This is likely attributable to the decomposition of carbonates formed at the surface. Again, the situation seen here is very different from that shown in Figs. 4a and 4b. Only O_γ appears to initially be populated for oxygen dosing pressures lower than 0.1 mbar. The desorption temperature maximum is initially about 1050 K. The O_γ signal here shows a maximum desorption temperature of 1073 K. The O_β species populates first at higher dosing pressures and the desorption maximum shifts again to lower temperatures for increasing dosing pressures. The O_β desorption temperature obtained for doses made in excess of 10 mbar is constant and is approximately the same as that observed for similar doses made at 773 K seen in Fig. 4b. The relative amount of O_β and O_γ produced is shown in the inset of Fig. 4c and exhibits yet another trend than seen in Figs. 4a and 4b. There are two obvious inflection points. The first appears slightly below 10^{-1} mbar O_2 and the second at 50 mbar O_2. Again, this variation suggests that the silver morphology has changed during the oxygen pretreatment. The variation at 973 K is, however, different than that seen in the inset of Fig. 4b for doses made at 773 K.

Interpretation of the TD Spectra

The observed trends for all dosing temperatures and pressures can be explained by taking into account the competing effects of pure thermal reordering of silver and oxygen-induced faceting. Dosing oxygen at 573 K resulted in no change in the relative amounts of O_β and O_γ formed as a function of dosing pressure hinting that the morphology remains unchanged. 573 K is apparently not sufficiently high to result in substantial mass transfer of silver. This temperature is approximately 200 K lower than the Tamman temperature which must be reached for the kinetics of silver interdiffusion to be fast enough to allow significant mass transport during the course of a typical experiment (9). This interpretation is supported by the fact that the desorption temperatures for O_β seen in Fig. 4a remains essentially constant as a function of the dosing pressure. This is in contrast to the strong pressure dependence of the temperature desorption maxima recorded after oxygen exposures made at 773 K. It is likely that changes in the silver morphology occur at this temperature.

The correlation of the desorption temperature with morphology is made possible by the fact that the temperature desorption maximum of a bulk-dissolved oxygen species should vary in proportion to the diffusion resistance. Higher desorption temperatures suggest higher diffusion resistance and vice versa. The observed decrease of the O_β desorption temperature with increasing dosing pressure indicates that the diffusion resistance decreases for increasing

oxygen pressures. It has been shown by *in situ* XRD that incorporation of oxygen into silver induces a distortion in the (110) silver planes which results in an optimum fit for oxygen diffusion in the silver bulk (14). The incorporation of oxygen into the silver lattice has also been shown to cause an increase in the unit cell constant for silver particles supported on alumina (30). Of the three dosing pressures used here, 773 K represents an optimum where oxygen-induced restructuring dominates over pure thermal reordering resulting in decreased diffusion resistance. The increased O_β desorption temperature for exposures made at pressures below 1.0 mbar seen in Fig. 4b results from the fact that pure thermal reordering kinetics dominate at low oxygen pressures. The decreased O_β desorption temperature obtained for increasing oxygen dosing pressures results again from the increased role of oxygen-induced restructuring at higher pressures. It is interesting to note that the maximum desorption temperature remains constant for all pretreatments made at pressures greater than 10 mbar. This implies that an equilibrium situation is attained at or above this pressure where the catalyst no longer undergoes restructuring.

The behavior seen in Fig. 4c provides a clear indication that increasing the dosing temperature to 973 K results in a situation where the thermal rearrangement of silver becomes the dominating process. This explains the fact that only O_γ is formed for dosing pressures lower than 0.1 mbar made at 973 K. Increasing the dosing pressure results in the same trend seen in Fig. 4b where oxygen-induced faceting causes the desorption maximum to shift to lower temperatures. This behavior cannot be explained by a simple second-order thermal desorption model as the species evolved originate from oxygen located in the bulk and not on the surface. Again, the desorption of oxygen is limited by the diffusive flux of O_β from the bulk to the surface.

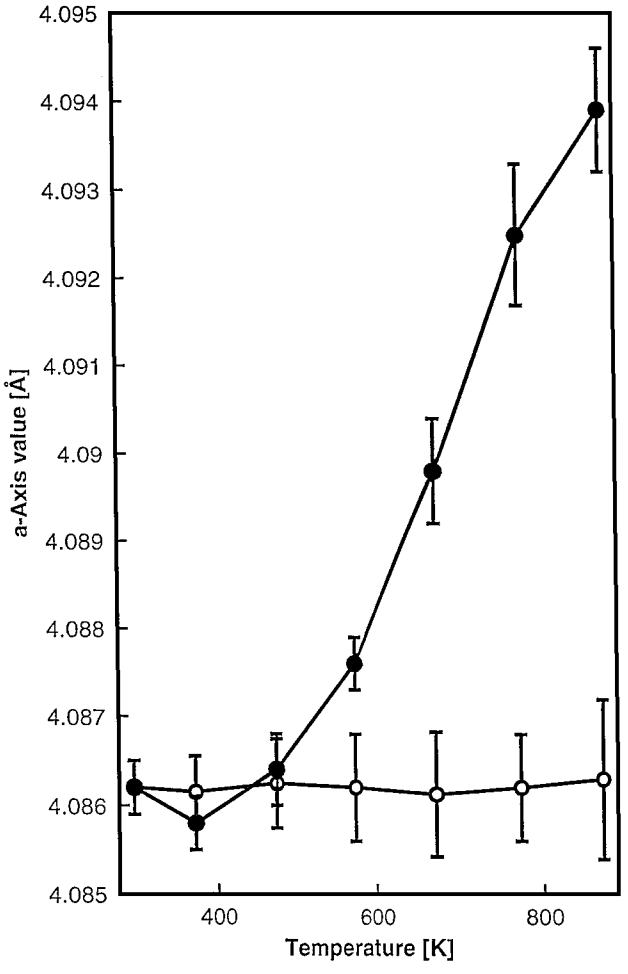

FIG. 5. Variation of the unit cell constant as a function of temperature under oxygen and methanol. The values have been corrected for the thermal expansion coefficient.

In Situ XRD Evidence for Bulk-Oxygen Dissolution

In situ analysis of silver powder was performed in order to gain information about bulk transformations occurring as a result of high-temperature treatment in oxygen. Measurements were made under a pure oxygen atmosphere as well as a 14% methanol in helium mixture. These represent the extremes of oxidation and reduction. Previous work (3, 14, 16, 17) has shown that methanol is an excellent reducing agent for silver. Measurements made in a methanol atmosphere function, therefore, as reference measurements. Figure 5 shows the results obtained for variations of the unit-cell constant as a function of temperature. The thermal expansion of silver was subtracted for both runs. Unit-cell expansion provides direct evidence for the incorporation of oxygen into the silver bulk. Oxygen is known to occupy octahedral holes in the fcc lattice of silver (5, 6). The direct determination of the oxygen positions by powder X-ray diffraction is, however, impossible as the X-ray scattering factor (f-factor) for silver dominates over that of oxygen in this low concentration regime ($C_{O2} < 100$ ppm). The onset of the unit cell expansion correlates excellently with the thermal desorption of O_β shown in Figs. 4a–4c. It is critical to note that no stoichiometric oxide is formed here. No additional reflections characteristic of stoichiometric silver oxides were found. The unit-cell expansion is, therefore, a secondary effect occurring as a result of the incorporation of oxygen into the bulk.

Figures 6a and 6b show the variation of the (111) and the (311) integral halfwidths as a function of temperature for both the oxygen and methanol runs. Figures 6c and 6d show the variation of the (220) and (200) integral halfwidths. The figures are grouped according to their respective zone axes. The zone axis represents the axis formed by the two intersecting planes shown. The increase of the integral halfwidth seen in Figs. 6a–6d at 573 K corresponds exactly with the onset of O_β desorption shown in Figs. 4a–4c and the increase in the unit-cell constant shown in Fig. 5. These

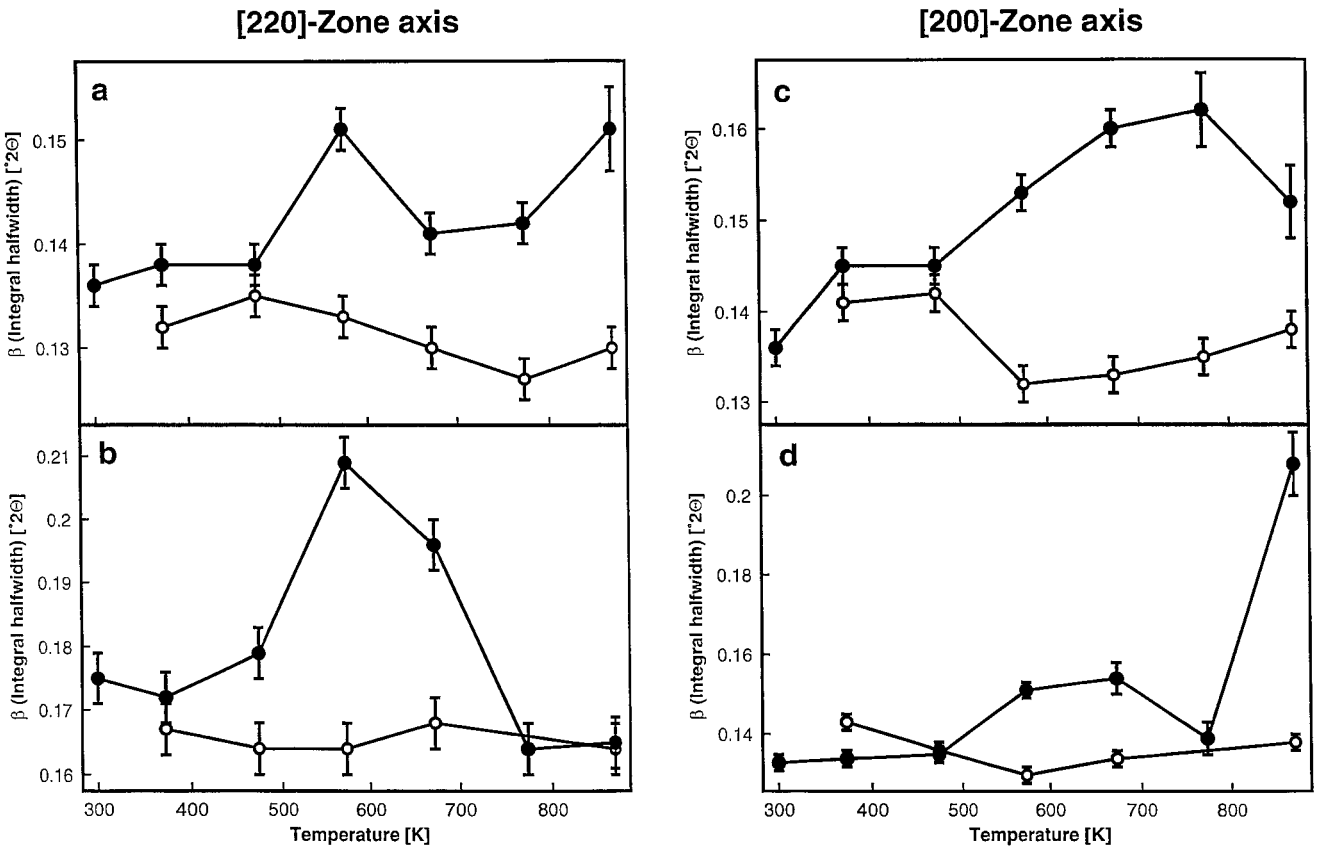

FIG. 6. Variations in β (integral halfwidth) as a function of temperature under oxygen and methanol for the silver reflections (a) (111), (b) (311), (c) (200), (d) (220).

variations result, therefore, from the diffusion of oxygen into the silver.

An increase in the integral halfwidth indicates the formation of defects or the building up of stress in the crystal lattice. The integral halfwidths of the reflections forming the [220] zone axis in Figs. 6a and 6b and the (220) plane in 6d vary in a similar way. The (200) reflection shows a different trend. A model which explains these qualitative trends is shown in Fig. 7a. The similar trends of the (111), (311), and (220) reflections indicates an increase of strain or a decrease in crystal size along the [110] direction (their common zone axis). This behavior is therefore a strong argument for the diffusion of oxygen along the [110] direction into the bulk. The decrease of the integral halfwidths of the (111), (311), and (220) reflections above 573 K and the increase of the (200) reflection indicates a reorganization of the anisotropic defect distribution caused by the diffusion of oxygen in the [110] channels.

Silver crystallizes in the fcc structure. The symmetry of the fcc structure implies that thermal expansion occurs isotropically. The incorporation of oxygen in the silver bulk introduces a degree of anistropic strain into the system which should result in the formation of long needle-like microcrystals. The formation of elongated crystals is a result of the fact that the atoms oriented along the a_1 vector ([110] direction) shown in Fig. 7a are not disturbed by the displacement of the face-centered atoms in the a_2 and a_3 vectors. The anisotropic development of internal stress results in the anisotropic recrystallisation of the silver into long crystals. Figure 7b is a ball model cut through the (110) surface showing the channels through which oxygen may diffuse. Diffusion is initially favored along the grain boundaries formed between the crystallites. At elevated temperatures, grain boundaries begin to anneal and the activation barrier for interstitial diffusion of oxygen in the crystal volume is overcome. The unit-cell constant increases as a result of the incorporation of oxygen into the silver leading to increasing stress between the microcrystalline domains. The accumulation of stress results in rupture and subsequent crack formation. The formation of more and larger crystal grains further enhances bulk diffusion hence speeding up the entire cycle. This is an autocatalytic process where incorporation of oxygen in the bulk results in an increased diffusivity for oxygen.

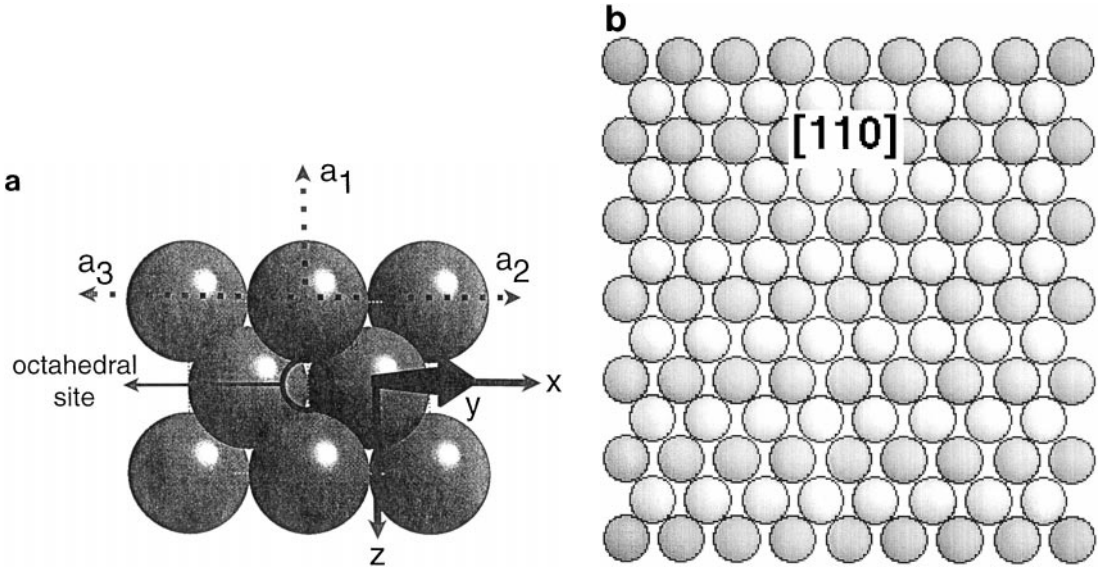

FIG. 7. (a) Ball model cut through the silver (110) plane. Suggested mechanism for oxygen-induced bulk restructuring. (b) Ball-model cut through the (110) plane showing the diffusion channels for oxygen.

STM Results

Figure 8 shows an STM image of the silver foil surface following treatment in a 10% O_2 atmosphere in helium. Large crystallites composed of smaller columnar crystallites are seen. The large crystals imaged with STM are similar to those found with SEM and are typically in the μm size range. The smaller crystallites vary in size and exhibit a surface roughness of approximately 3–5 nm. This image is typical of images taken at almost every point on the surface.

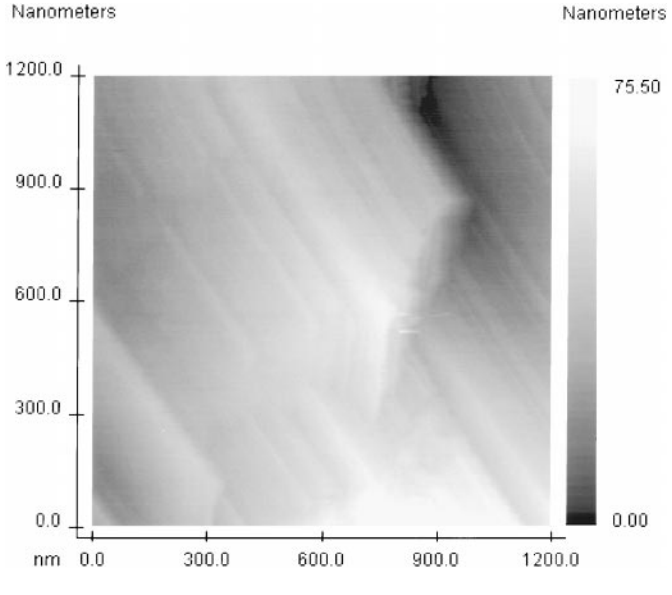

FIG. 8. Scanning tunneling microscroscopy image of a silver foil pretreated in 10% O_2 for four days.

The main difference in the scans is the orientation of the μm-sized crystal structure formed. In all cases, the large crystals are composed of columns of smaller microcrystals. This confirms the previous model derived on the basis of the XRD data.

TDS and XPS Evidence for Surface Diffusion Inhibition

The idea that O_γ is formed by segregation of O_β to the surface via interstitialcy diffusion through densely packed crystalline planes was tested. The sample was heated to 873 K in vacuum for 30 min. This vacuum treatment results in extensive annealing as well as the formation of densely packed terminating surface structures (i.e., (111)) (18). These structures should offer increased resistance to oxygen diffusion. TDS and XPS analysis were performed on the sample prior to and after this vacuum treatment. TDS provides information about the thermal stability of all oxygen species present in the bulk whereas XPS provides chemical information about species located in the near-surface region (approx. 30 Å). With this combined information, one can effectively differentiate between processes occurring in the bulk and near-surface regions.

A typical spectrum with subsequent peak deconvolution and species assignments is shown in Fig. 9. O_β is assigned to the peak centered at 531 eV and O_γ to the peak centered at 529 eV (16). The large FWHM for O_β relative to O_γ supports the argument proposed earlier, based on the TDS spectra, that O_β is bulk-dissolved oxygen located both in the grain boundaries as well as in crystallites of various orientations. The resulting heterogeneity of the O_β electronic environment results in a broadening of the XPS

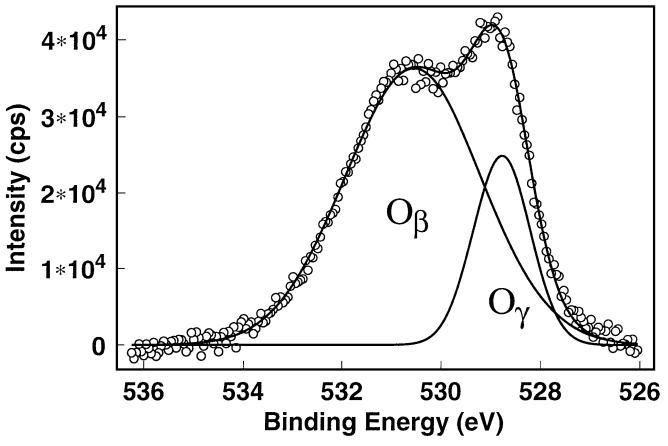

FIG. 9. X-ray photoelectron spectra for silver pretreated in 100 mbar O_2 at 873 K.

signal (Fig. 9) as well as the TDS signal (Figs. 4a–4c). There is also an overlap of the two signals which likely results in an increase of the observed O_γ signal.

The results of both the TDS and XPS experiments are combined and are shown in Fig. 10. It is immediately obvious that treatment of the silver in vacuum prior to oxygen dosing results in a drastic change in the O_β/O_γ ratio detected by TDS. O_γ usually accounts for about 20% of the thermal desorption signal under these conditions. Dosing oxygen subsequent to having treated the sample in vacuum results in a fourfold increase of the integrated O_γ intensity (relative to an O_2-equilibrated sample), which now represents more than 80% of the total desorption signal.

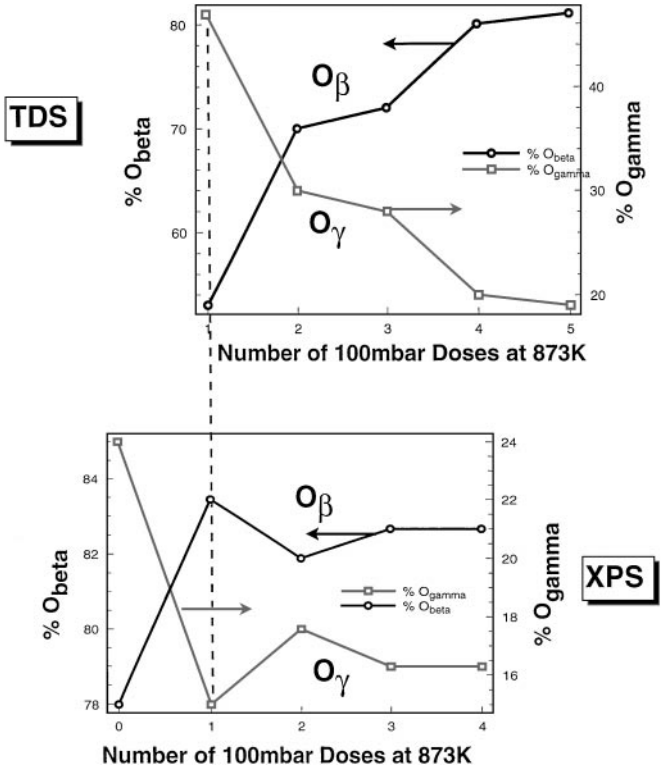

FIG. 10. Comparison of the integrated intensities for O_β and O_γ obtained from thermal desorption spectra and X-ray photoelectron spectra of silver initially treated for 30 min at 873 K in vacuum then subsequently dosed with 100 mbar O_2 at 873 K.

Figure 10 shows that continued exposure to oxygen eventually returns the surface to its original state where O_β is the dominant signal. The changes of the relative XPS intensities clearly indicate that the drastic variation of the TDS oxygen desorption signals seen in the upper half of Fig. 10 results from partial blocking of O_β segregation to the surface. This occurs as a result of the surface restructuring during the vacuum pretreatment.

There is a large decrease of both the O_β (531 eV) and O_γ (529 eV) signal intensities immediately following the vacuum treatment (first point prior to O_2 exposure in XPS). The silver is depleted of most of the O_β which results in O_γ being the dominant signal at this point (exhibits the highest thermal stability). Subsequent dosing of oxygen shows a slight increase of the XPS signal for O_β relative to O_γ. The O_γ signal observed in XPS is assigned to oxygen intercalated in the uppermost silver layers. The fact that the integral O_γ signal intensity observed with XPS does not show the same trend as observed by TDS arises from the fact that oxygen located deeper in the silver bulk is not observable using XPS. This must be taken into account when assigning species observed by both techniques. The integral O_γ desorption signal observed by TDS represents the total flux of oxygen contained in the bulk which diffuses through low-indexed crystalline planes formed at the surface during the pretreatment or during the TD experiment itself. XPS shows, essentially, a snapshot of the surface subsequent to pretreatment. Therefore, the O_γ observed by XPS is equivalent to the O_γ observed by TDS only in that moment when the oxygen has segregated from the bulk into the uppermost atomic layers of silver where it may be detected. Extreme caution must be used when interpreting spectra attributed to subsurface species. The integral areas of O_γ and O_β measured by both XPS and TDS agree excellently after having repeatedly exposing the silver to oxygen ($O_\beta = 84\%$, $O_\gamma = 16\%$). These values represent the values expected after the silver has equilibrated with the surrounding gas atmosphere. The similarity of the values obtained with both methods indicates that O_γ is confined to the uppermost silver layers under equilibrium conditions. The fact that O_γ is located only in the uppermost layers results, therefore, from the fact that close-packed terminating crystal structures are formed at elevated temperatures which subsequently hinders segregation of bulk-dissolved oxygen to the surface and forces oxygen to diffuse through the crystal lattice.

ISS-Evidence for a Concentration-Dependent Diffusion Constant and Surface Diffusion Inhibition

Further evidence supporting the above-mentioned interpretation was obtained by performing ion-scattering-spectroscopy (ISS). The first run was made after dosing 100 mbar O_2 at 873 K subsequent to having equilibrated the sample by repeatedly dosing with oxygen at 100 mbar and 873 K (analogous to the TDS/XPS experiment). The concentration profile represents essentially the same situation as that found after having performed multiple oxygen exposures (Fig. 10). A second run was made by first heating in vacuum at 873 K and then dosing once at 100 mbar O_2 and 873 K. The normalized results are shown in Fig. 11. A comparison of these runs reveals that surface annealing results in a surface diffusion barrier to the segregation of oxygen from the bulk. The oxygen concentrations in the near-surface region are identical for both runs. The variation of the total oxygen content as a function of depth is, however, very different for both pretreatments. The concentration-depth profile distribution for the oxygen-equilibrated sample shows a gradual decrease in the oxygen signal as a function of depth. The sample subjected to vacuum treatment prior to oxygen dosing shows an initial steeply dropping slope which eventually plateaus at greater depth. Bulk-dissolved oxygen was obviously forced into a thin layer in the near-surface regime during segregation as a result of the formation of the diffusion barrier formed during vacuum annealing. The form of the depth profile also yields important information. In this case, the 0.1-mm thick silver foil is approximated as a semi-infinite medium subjected to the initial boundary conditions $C(O_2)_{x=0} = S_{O2} \times P(O_2)$, $C(O_2)_{x=1/2L} = 0$. S_{O2} is the solubility of oxygen in silver and $P(O_2)$ is the gas phase oxygen pressure. Normal Fickian diffusion predicts a linear decrease in oxygen concentration as a function of depth (6, 9, 19). The nonlinearity of the concentration-depth profile provides strong evidence that the diffusion coefficient is concentration dependent. The concave-up curve form indicates that the diffusion coefficient is a positive function of oxygen concentration. This agrees excellently with the supposition that oxygen induces a recrystallization of the bulk at elevated temperatures, which subsequently results in an enhancement of oxygen diffusion. It is to be expected, therefore, that oxygen diffusion is favored for those parts of the silver bulk which have incorporated the largest amount of oxygen (O_β) and therefore are the most strongly distorted (high O_β concentration).

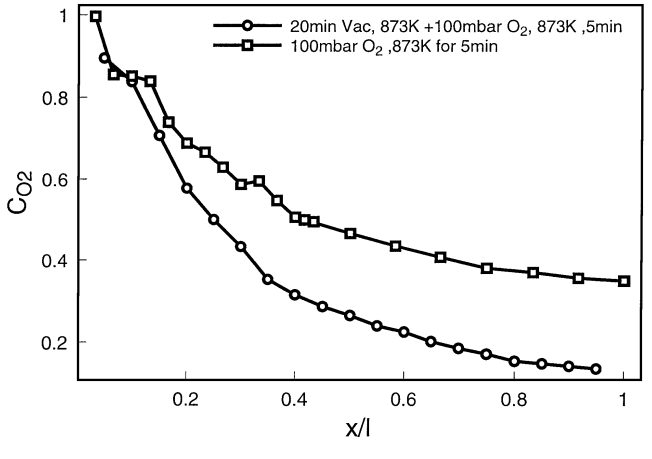

FIG. 11. Results of depth profiling analysis obtained with He^+ ion-scattering spectroscopy of silver equilibrated with oxygen (open squares) and silver dosed with oxygen subsequent to heating in vacuum (open circles).

It is absolutely critical to stress the fact that the high temperatures necessary for activation of interstitialcy diffusion will always lead to the formation of densely packed terminating surface surfaces. This explains the fact that O_γ has only been observed in the (111) terraces of silver and appears to occupy only the uppermost silver layers (16, 31) under equilibrium conditions. An exact determination of the diffusion mechanisms involved obviously requires further investigation but the arguments presented here provide strong evidence for the presence of both diffusion mechanisms (interstitial and interstitialcy). High-temperature restructuring is expected to be a problem encountered by any group attempting to determine the kinetics of solid-state diffusion at elevated temperatures. Extrapolation on the basis of activation energies and pre-exponential factors obtained at lower temperatures might be a solution to this problem. As seen here, however, the temperatures at which the diffusion of a gas in the solid is activated occur simultaneously with the temperature at which restructuring of the solid begins. Quantitative determination of diffusion kinetics as a function of crystallite orientation is, therefore, a challenging problem which is far from being solved.

It is worth commenting on the assignment of the O_β and O_γ peaks (Figs. 4a–4c) to a bulk-dissolved and surface-intercalated species. This seems, at first glance, contradictory. Common sense would dictate that a species located in the near-surface region would diffuse before a bulk dissolved species. It is critical, however, to understand that the silver–oxygen system is in a dynamic state of change during the course of a TDS measurement. The silver morphology and oxygen concentration profile change during the course of the measurement. The oxygen-induced restructuring is reversed upon heating in vacuum at the same time at which oxygen is diffusing and desorbing from the sample. The fact that the surface restructures to close-packed crystalline faces at elevated temperatures combined with the depletion of bulk oxygen during the TDS run results in the minimum seen in all runs at approximately 900 K (Figs. 4a–4c). The surface is essentially annealed shut during the TDS run. The diffusion mechanism shifts from interstitial to interstitialcy

diffusion above this temperature. Only then can oxygen desorb through the tightly packed crystal structures formed upon annealing. This results in the O_γ peak. The TDS runs performed here are far removed from the more traditional "static" conditions typical of lower temperatures, Langmuir dosing on single-crystalline substrates. This results in an interpretation which is perhaps unorthodox with respect to traditional surface-science thinking but is necessary to a correct interpretation of this surprisingly complex system.

CONCLUSIONS

Two distinctly different types of subsurface atomic oxygen are formed in oxygen-pretreated, polycrystalline silver. The first is termed O_β and refers to bulk-dissolved oxygen which diffuses along grain boundaries or via interstitial hole-jumping through loosely packed surface crystalline planes. The second is termed O_γ and is formed at elevated temperatures under conditions at which interstitialcy diffusion is likely to be possible and results in the substitution of silver atoms by oxygen. The catalytically active O_γ species is essentially O_β in that moment when oxygen segregates from the bulk to the surface via volume diffusion of oxygen through low-indexed terminating crystalline planes. Formation of both species is a strong function of temperature and oxygen pressure. The interaction of oxygen with silver results in a substantial decrease in the diffusion barrier for oxygen pressures in the range of $1.0\ \text{mbar} < P_{O2} < 10\ \text{mbar}$. This effect is caused by oxygen-induced recrystallization which leads to the formation of more open surface crystalline planes, a reorientation of the facets, and the distortion of the unit cell forming channels in the [110] direction through which oxygen may diffuse. Dosing at pressures above 10 mbar O_2 leads to a gradual increase in the barrier to oxygen diffusion. This is due to a texturing of the facets to a predominantly (331) terminating surface. This study lays the groundwork for understanding the role played by these oxygen species in silver-catalyzed oxidation reactions at elevated temperatures. The strong dependence of oxygen diffusion kinetics on morphology is expected to have a direct impact on the reaction kinetics of the oxidative coupling of methane, which is believed to be catalyzed by O_γ. A comparison of OCM reaction kinetics with O_2 diffusion kinetics in silver will be presented in a subsequent publication.

REFERENCES

1. Ullman, *in* "Ullman's Encyclopedia of Industrial Chemistry," 5th ed., Vol. A11, pp. 619–651, VCH Verlagsgesellschaft, Weinheim, 1988.
2. Sperber, H., *Chemie-Ing.-Tech.* **41** (17), 962 (1969).
3. Lefferts, L., van Ommen, J. G., and Ross, J. R. H., *Appl. Catal.* **31**, 291 (1987).
4. van Santen, R. A., and Kuipers, H. P. C. E., *Adv. Catal.* **35**, 265 (1987).
5. Anshits, A., Shigapov, A., Vereschchagin, S., and Shevin, V., *Catal. Today* **26**, 601 (1990).
6. Eichenauer, W., and Pebeler, A., *Z. Metallkade.* **48**, 373 (1957).
7. Outlaw, R. A., Wu, D., Davidson, M. R., and Hoflund, G. B., *J. Vac. Sci. Technol. A* **10**, No. 4, 1497 (1992).
8. Rovida, G., Pratesi, F., Maglietta, M., and Ferroni, E., *Surf. Sci.* **43**, 230 (1974).
9. Backx, C., de Groot, C. P. M., and Biloen, P., *Surf. Sci.* **104**, 300 (1981).
10. Schmalzried, H., *in* "Chemical Kinetics of Solids," VCH Verlagsgesellschaft, Weinheim, 1995.
11. Wei, Ta-Chin, and Phillips, J., *Adv. in Catal.* **41**, 359 (1995).
12. Bao, X., Barth, J. V., Lempfuhl, G., Schuster, R., Uchida, Y., Schlögl, R., and Ertl, G., *Surf. Sci.* **284**, 14 (1993).
13. Bonnel, D. A., *in* "Scanning Tunneling Microscopy and Spectroscopy, Theory, Techniques and Applications," VCH, Weinheim/New York, 1993.
14. Stranski, I. N., and Krastanov, L., *Sitzungsber. Akad. Wissenschaft Wien* **146**, 797 (1938).
15. Herein, D., Nagy, A., Schubert, H., Weinberg, G., Kitzelmann, E., and Schlögl, R., *Z. Phys. Chem.* **197**, 67 (1996).
16. Somorjai, G. A., *in* "Introduction to Surface Chemistry and Catalysis." Wiley, New York, 1994.
17. Bao, X., and Deng, J., *J. Catal.* **99**, 391 (1986).
18. Bao, X., Muhler, M., Schedel-Niedrig, Th., and Schlögl, R., *Phys. Rev. B* **54**, 2249 (1996).
19. Schubert, H., Tegtmeyer, U., Herein, D., Bao, X., Muhler, M., and Schlögl, R., *Catal. Lett.* **33**, 305 (1995).
20. Bowker, M., Barteau, M. A., and Madix, R. J., *Surf. Sci.* **92**, 528 (1980).
21. Backx, C., de Groot, C. P. M., Biloen, P., and Sachtler, W. H. M., *Surf. Sci.* **128**, 81 (1983).
22. Sexton, B. A., and Madix, R. J., *Chem. Phys. Lett.* **76**, 294 (1980).
23. Boronin, A. I., Bukhtiyarov, V. I., Vishnevskii, A. L., Boroskov, G. K., and Savchenko, V. I., *Surf. Sci.* **210**, 195 (1988).
24. Engelhard, H. A., and Menzel, D., *Surf. Sci.* **57**, 591 (1976).
25. Barteau, M. A., and Madix, R. J., *Surf. Sci.* **140**, 108 (1984).
26. Chalmers, B., King, R., and Shuttleworth, R., *Proc. R. Soc. A* **193**, 465 (1948).
27. Hondros, E. D., and Moore, A. J. W., *Acta Metall.* **8**, 647 (1960).
28. Rhead, G. E., and Mykura, H., *Acta Metall.* **10**, 843, 578 (1962).
29. Czanderna, A., Chen, S., and Biegen, J., *J. Catal.* **33**, 163 (1974).
30. Yanase, A., Komiyama, H., and Tanaka, K., *Surf. Sci. Lett.* **226**, L65 (1990).
31. Herein, D., Werner, H., Schedel-Niedrig, Th., Nagy, A., Bernd, S., and Schlögl, R., "Proc. 3rd World Congress on Oxidation Catalysis, Sept. 21–26, 1997" (S. T. Oyama *et al.*, Eds.), Elsevier Science, Amsterdam, 1997.